A CONTROL STRATEGY TO EMULATE INERTIA THROUGH GRID-FOLLOWING INVERTER

Yuri Roberto Ferreira, Rodrigo Trentini, Rüdiger Kutzner
Instituto Federal de Santa Catarina
Câmpus Jaraguá do Sul – Rau – Curso de Bacharelado em Engenharia Elétrica
e-mail: yuri.f@aluno.ifsc.edu.br, rodrigo.trentini@ifsc.edu.br, ruediger.kutzner@hs-hannover.de
Trabalho de Conclusão de Curso – TCC – 18/08/2021

***Abstract* – The concern for the environment and the actual economic situation result in the growing search for renewable means of energy generation. However, renewable sources of electrical energy interfaced by inverters do not have the same inertia and damping that exists in synchronous machines from conventional energy systems, such as thermal. The lack of inertia resulting from the high level penetration of renewable energies can lead to increased frequency excursions and, consequently, to system instability. Among the various studies aimed at reducing this unwanted effect, there is a proposal to emulate inertia through inverters and their control [1]. In this study, it is suggested the development and application of a control strategy to emulate inertia through a grid-following inverter. After simulations in a system with solar photovoltaic energy generation connected to a grid with infinite bus, results show the effectiveness of inverter control with virtual inertia.**

***Keywords* – Grid-following inverter, virtual inertia, renewable sources, electric power system stability.**

I. INTRODUCTION

In recent decades, the growing concern with the environment, the economic movement related to new technologies and the global energy crisis have led to an increase of renewable energy sources utilization. Thus, the electricity sector and its demand is one of the fastest growing in the energy mix, which is why the penetration of energy sources such as solar photovoltaics (PV) and wind is constantly increasing in electric power systems (EPSs) [2]. Some countries such as Germany, Denmark and Ireland have presented more than 20% of penetration of those renewable sources in past years [3]. This fact originates a concern about the system stability, especially frequency stability, once solar PV and wind energy sources are interfaced by inverters and unprovided of natural rotational inertia and damping [4]. Two significant events highlight the importance of ensuring frequency stability: the blackout in Australia in 2016 and the power cut in the UK in 2018 [5].

Large frequency variations can compromise the safe operation of the system due to mechanical limitations of individual synchronous machines, protection devices triggered by frequency variation limit or timing problems related to load shedding. After disconnection of any generator or load in a system, the rate of change of frequency (RoCoF) is practically instantaneous due to the action delay of any control, which represents the greatest amplitude of the frequency variation. However, large levels of inertia can reduce this initial variation amplitude [6].

The intrinsic rotational inertia of synchronous machines (SGs) contained in conventional eletric power sources, such as thermal and hydroelectric, and the damping of its governors assure that systems remain stable in case of faults, fluctuation of power injections, load variations and frequency deviations [7]. When frequency deviation occurs in an EPS, the inertia of the synchronous machine is the first to act, supplying or absorbing kinetic energy from the system. However, sources interfaced by converters do not have this feature.

Many researches were carried out with the objective of finding ways to mitigate losses resulting from the deficiency of inertia and damping in EPSs. A very studied manner is the use of converters that mimic the action of the synchronous generator. These converters can apply virtual inertia (VI) in low-inertia generation systems [1]. As converters operate at faster frequencies, it is possible that they mimic the primary control response of synchronous generators [8].

Therefore, the aim of this paper is to demonstrate and validate a control strategy of a VI-based inverter with inertia emulation in a PV solar energy generation system interconnected to an EPS with infinite bus. In this case, the infinite bus represents a system with a high level of inertia provided by synchronous generators and the inverter must be able to compensate for small frequency deviations in the grid through its primary control to mitigate the frequency instability.

This paper is structured as follows: In Section II, the main types of inverters based on virtual inertia control are presented, including the inverter adopted in this study. The fundamental concepts of power transfer, especially the swing equation, which presents the main concept for inertia emulation in this case, are demonstrated in Section III. In Section IV, the structure of the grid-following inverter with inertia emulation is presented, containing the power and current control system, the basic procedure of synchronization with the grid and the implementation of inertia emulation control. The electrical system model used to collect the results through simulations is shown in Section V, as well as the applied renewable energy

generation data. In Section VI, the methodology of the tests applied in simulations is demonstrated, as well as the analysis of the results. Finally, Section VII presents the final considerations and proposals for future implementations.

II. GRID-CONNECTED VI-BASED INVERTERS

The VI-based inverters are DC-AC converters that are originally developed based on the mathematical model of synchronous machines, which can be found in textbooks [9]. Consequently, a conventional converter with inertia emulation aims to reproduce the dynamics of a synchronous machine, as illustrates Fig. 1. Then, these converters are denominated virtual synchronous machine (VSM) or virtual synchronous generator (VSG) [10].

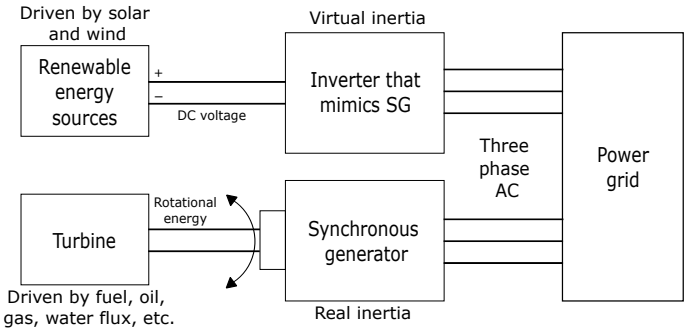

Fig. 1. Equivalence between VI-based inverter and synchronous machine.

Basically, the large number of inertia emulator types are separated into two categories: grid-following (GFL) and grid-forming (GFR). A grid-following inertia emulator device acts in frequency control injecting active power proportional to the frequency deviation and RoCoF in the grid. In contrast, the grid-forming inertia emulator is a voltage source that compensates for the imbalance between the consumed and generated power by changing the generated frequency [11].

These two types of VI-based inverters can be implemented in the same physical location on the system, although they function differently. The main implementation difference is in the VI emulation algorithm. A general connection of grid-connected solar PV and wind energy with VI-based inverter is shown in Fig. 2.

However, GFR and GFL inverters have some different application characteristics. The GFR inverter can operate both in micro and standalone grids, as it supports and generates its own frequency. For this reason, it is capable of containing higher-level frequency deviations. In addition, the GFR inverter acts as a voltage source and supplies active and reactive power to the grid. However, the GFR inverter has the slowest response due to the high inertia and its implementation is more complex [10].

Differently, the GFL inverter can not act in isolation, it always needs to have some other generator (or group of generators) that

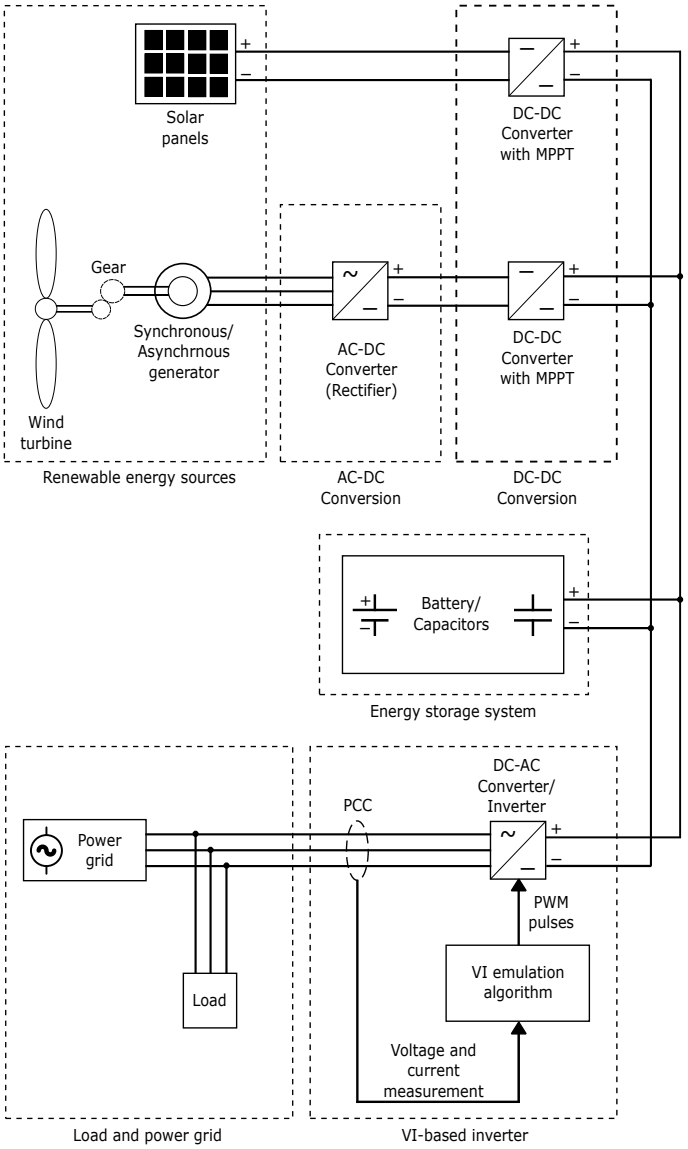

Fig. 2. General system with renewable energy sources and VI-based inverter.

imposes frequency connected at the same grid, as it follows the imposed frequency. The GFL acts as a current source that injects active and reactive power into the grid without imposing its frequency. However, GFL provides faster response to intermittent renewable energy generation and load variations. In addition, its design and implementation are more simplified, which makes it the most applied inverter in renewable energy generation systems interconnected to microgrids [10]. As GFL has a simpler and more common application, the objective of this study is its application in a solar energy generation system with inertia emulation connected to a microgrid.

The concept of inertia emulation in this study originates from the definition of power transfer equations and, especially, from the swing equation, which is exploited in the next section.

III. SWING EQUATION AND POWER TRANSFER EQUATIONS

The stability of the electrical power system is associated with three definitions: rotor angle, voltage magnitude and frequency stability [12]. Therefore, inertia emulation in grid-following inverters aims to act in the frequency stability control, more specifically in the primary frequency control of the power grid. In this case, this type of VI-based inverter is capable of controlling its power injection into the grid and compensating for small frequency disturbances. The reason why the power injected into the grid influences the frequency control is demonstrated by the swing equation.

The power transfer between synchronous machines and the electrical grid is the principle of the concept that involves the swing equation. Synchronous machines driven by a prime mover, such as a thermal turbine, generate a rotational magnetic field in the rotor that induces voltage in the machine's stator winding. The frequency of the induced voltage will be defined in the grid according to the machine rotational frequency, as the electrical frequency is synchronized with the rotational frequency of the rotor. Therefore, if the grid frequency is fixed at, e.g., 60 Hz, the output frequency of the synchronous machine must be equal in steady state. However, the torque unbalance due to the change of frequency in the power grid, or in the machine, generates an acceleration or deceleration, as demonstrated by equation (1) [13].

$$\tau_a = \tau_m - \tau_e, \tag{1}$$

where τ_a is the acceleration torque, τ_m is the mechanical torque applied by the synchronous machine and τ_e represents the electrical torque applied by the grid. The electrical torque is caused by the application of any load next to the generator or in the power grid. Considering that the rotor is a rigid mass with significant mass, the acceleration torque can be rewritten as

$$J\frac{d\omega}{dt} = \tau_m - \tau_e, \tag{2}$$

where J represents the moment of inertia of the synchronous machine and turbine rotor together and ω is the angular velocity of the rotor. This is the equation known as simplified swing equation [13]. As a consequence, the acceleration described by the time derivation of ω is the previously cited RoCoF. According to [12], the product of nominal angular velocity and torque results in power. Furthermore, torque and power in per unit (pu) are the same. Hence the equation can be rewritten as follows.

$$J\frac{d\omega}{dt} = \frac{P_m}{\omega} - \frac{P_e}{\omega}, \tag{3}$$

where P_m is the power supplied by the generator shaft and P_e is the electric power of the grid, both in W. Though, it is very common to write the swing equation in pu base where the constant of inertia H is given in seconds, according to equation (4).

$$H = \frac{1}{2}\frac{J\omega_s^2}{S_{base}}, \tag{4}$$

where S_{base} is the system base power value and ω_s is the synchronous angular velocity. In this case, H is a constant that quantifies the kinetic energy of the rotor at synchronous speed in terms of how many seconds it takes the generator to supply the amount of energy equivalent to the grid energy. Therefore, the time it takes the rotor to reach synchronous speed (T_m) is given by equation (5).

$$T_m = \frac{J\omega_s^2}{S_{base}} = 2H \tag{5}$$

Finally, considering powers and velocity values in per unit (pu), the terms from equation (5) are substituted into equation (3) and the power transfer equation is given.

$$2H\frac{d\omega}{dt} = P_m - P_e \tag{6}$$

Through the analysis of equation (6), it is verified that the terms on the left side of the equality represent the power resulting from the acceleration of the synchronous machine when there is an imbalance between generated and consumed power. This imbalance results in the oscillation of the grid frequency and the product $2H$ denotes how the machine inertia influences the dynamics of the grid frequency variation.

IV. IMPLEMENTATION OF GRID-FOLLOWING INVERTER WITH INERTIA EMULATION

A grid-following VI-based inverter must be able to emulate the inertia equivalent of a synchronous machine with the same inertia constant H.

Most of the converters used today are the grid-following type. A GFL inverter is a voltage source converter (VSC) that acts as a current source and injects active and reactive power into the grid according to the desired power or current reference [14]. To inject power into the grid, it is necessary to use the phase-locked loop (PLL) in the control system to measure the voltage angle and synchronize with the grid.

Before the implementation of virtual inertia algorithm, it is necessary to implement the GLF inverter control structure.

A. GFL inverter control system

The GLF inverter injects power into the grid according to active P_{ref} and reactive Q_{ref} power references provided by the secondary frequency control. For this, power control is performed and then current control generates the voltage signal for the frequency inverter switching system. First, it is necessary to measure the three-phase voltage v_{abc} and current i_{abc} on the inverter output bus [14]. This measuring point is called the point of common coupling (PCC). The GFL inverter control scheme

implemented in this study is shown in the Fig. 3.

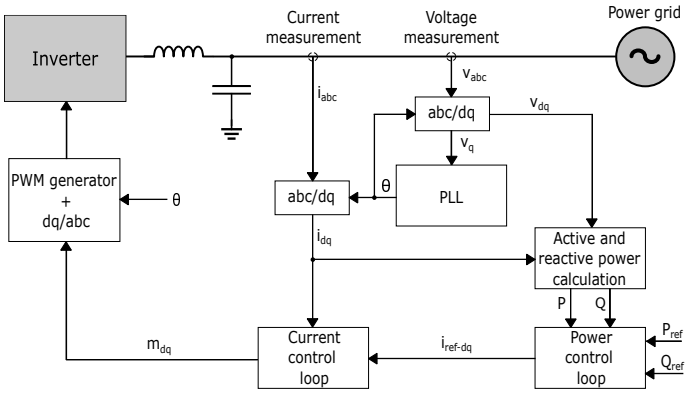

Fig. 3. Grid-following inverter control schematic.

The power control loop has two inputs, which one receives the power references values provided by the secondary frequency control and the other receives the calculated power based on voltage and current measurements from inverter output bus or PCC. Thus, the controller, which is usually a PI controller, generates the reference current signal i_{ref-dq} for controlling the current.

In order to generate the reference signal m_{dq} for the inverter PWM port, the current control loop has as inputs the reference signal generated by the power controller and the current measured at the PCC. Also, it is common to use a PI controller in the current controller. Finally, the inverter supplies the grid with the necessary current level and angle to inject the desired active and reactive power.

However, the controllers by themselves do not ensure the synchronization between the voltage generated by the inverter and the grid voltage. The synchronization occurs due to the application of *Park's transformation* algorithm and estimation of the voltage angle and frequency performed by the PLL.

B. GFL inverter synchronization

A GFL inverter uses synchronous reference also known as *dq*-based frame to ensure synchronization with the grid. In this way, the PLL measures the voltage angle θ used in the transformation of the three-phase voltage and current (*abc*) to direct-quadrature-zero (*dq*0) [15]. By knowing the voltage phase angle and the voltage and current amplitudes ($|v|$ and $|i|$), it is possible to control power and current using just the 2 axis reference instead of 3. The *abc*-*dq*0 transformation is known as *Park's transformation*, just as *dq*0-*abc* transformation is the inverse *Park's transformation* [12]. After the current control, PWM reference signal is transformed to *abc* frame again.

Once GFL inverter control, measurements and synchronization structure are implemented, the inertia emulation algorithm can be added.

C. Inertia emulation control

The application of inertia emulation is based on swing and power transfer equations (see Section III). Then, the GLF inverter must be able to compensate for frequency variations by injecting active power into the grid. According to the swing equation (6), virtual inertia control needs the actual frequency value measured by the PLL to calculate the RoCoF and emulate mechanical power variation resulting from the generator inertia [16]. So, the VI control has as its output a power variation signal resulting from the action of the emulated inertia to compensate for the variation in RoCoF, as shown in equation (7).

$$P_{VI} = 2H\frac{d\omega}{dt} = P_m - P_e \tag{7}$$

As the goal is to inject active power proportional to RoCoF changes during frequency transients, VI controller does not act and the PLL does not need to be taking measurements in steady state. Also, the reactive power reference is always kept in zero in this case, because it does not affect inertia control. Fig. 4 illustrates the VI control diagram.

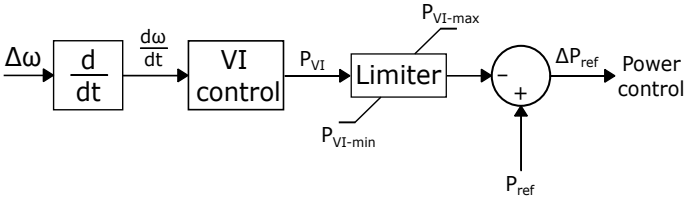

Fig. 4. Inertia emulation control diagram.

Thusly, P_{VI} signal is subtracted from power reference P_{ref} value provided by the secondary frequency control, resulting in a new active power generation reference signal ΔP_{ref}.

The VI control transfer function is given by equation (8).

$$C_{VI}(s) = \frac{K_{VI}}{sT_{VI}+1}, \tag{8}$$

where K_{VI} is the gain equivalent to the $2H$ inertia constant and T_{VI} is the VI controller time constant. However, it is important to have limitations on the power signal provided by inertia control, because when high-level frequency variations occur, the power control will receive either very high or very low power reference values which might lead the grid to instability.

V. GRID MODEL

A single machine infinite bus (SMIB) system is the standard EPS for stability analysis in relation to load variations, generated power reference changes, etc [17]. SMIB models use a synchronous generator connected to a transmission line, which connects to the infinite bus. Such EPS, although simple, helps to understand the influence of the dynamics involved, the power flow and other related phenomena. To maintain such structure, it is suggested to use an adapted SMIB in this study, where instead

of a synchronous generator, there is a solar PV generation with inverter system. Therefore, an EPS modeled as a typical North American distribution system [18] was considered and adapted to emulate inertia. The single-line diagram of the simulated model is illustrated in Fig. 5.

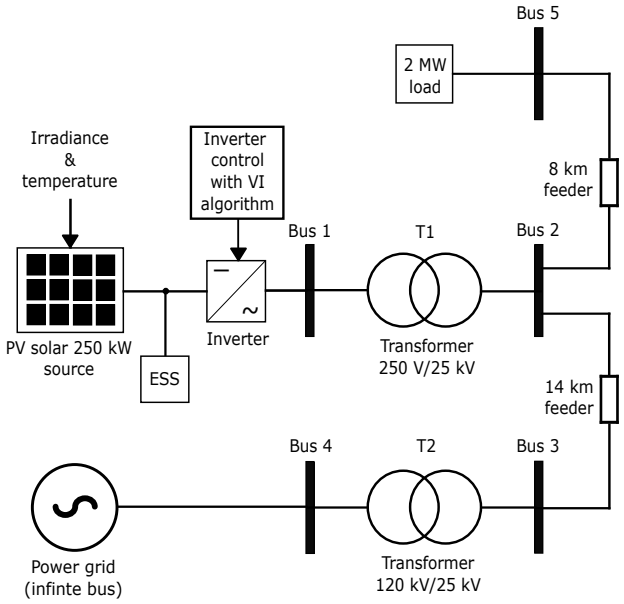

Fig. 5. PV solar source grid-connected system model.

The model adaptation involves the following changes to the original model: removal of the load of 30 MW and 2 MVAr, removal of the grounding transformer, inclusion of the system for changing the load of 2 MW and changes of the inverter control according to the schematic demonstrated in Fig. 3. plus the inertia control shown in Fig 4.

This EPS includes a PV solar farm that has nominal power of 250 kW connected to a three-phase voltage transformer $T1$ from 250 V (Bus 1) to 25 kV (Bus 2) at frequency of 60 Hz. Two feeders are connected at the Bus 2: a 14 km feeder connected to the Bus 3 and a 8 km feeder connected to the Bus 5. Between Bus 3 and Bus 4 there is a voltage transformer $T2$ from 25 kV to 120 kV. The infinite bus has 2500 MVA and 120 kV, which is connected at the Bus 4. Finally, a 2 MW load is connected at Bus 5.

A. PV solar farm

Photovoltaic solar energy has some advantages and disadvantages. The main advantages are: clean energy source, application mobility and low maintenance cost. Disadvantages include: high initial cost, weather dependence and large space occupation.

The implemented PV solar farm is composed by PV modules from Sun Power manufacturer, model SPR-415E-WHT-D. Each module has 128 cells, maximum power of 414.8 W and maximum voltage of 72.9 V with load [19]. Thus, the farm contains 88 strings in parallel with 8 modules in series each, guaranteeing a maximum power of approximately 292 kW and maximum output DC voltage of 583 V. As the nominal power is 250 kW, there is a margin in case of variations in solar irradiation, temperature, transient peaks and other factors that result in the intermittence of this form of generation. The DC voltage is regulated by a DC-DC converter with maximum power point tracking (MPPT) control, before the energy storage system (ESS). The ESS is composed of capacitors with a total capacitance of 100 mF and a set of batteries. The battery pack used has a nominal voltage of 500 V and a discharge rate of 1000 Ah. After the ESS, the DC voltage is converted by a three-phase inverter.

Considering that the performance of solar modules is affected by solar irradiance S (in W/m^2) and temperature T (in °C), Fig. 6 shows the performance curves of the adopted solar PV farm according to temperature variation. Also, performace curves considering irradiance variation are shown in Fig. 7.

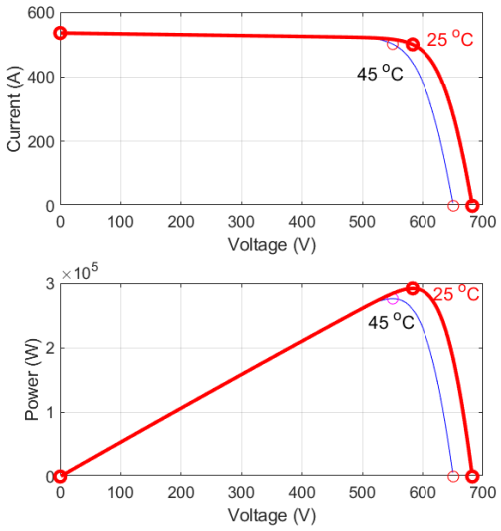

Fig. 6. PV farm performance curves according temperature variation.

The performance comparison between temperatures of 25°C and 45°C considers a average incident irradiation of 1000 W/m² on the modules (see Fig. 6). It can be seen that maximum power of 292 kW at the voltage of 583 V is reached at 25°C. Efficiency is lower at 45°C, reaching 276 kW at 550 V.

In Fig. 7, a performance comparison of the PV farm is performed with the irradiations of 100, 500 and 1000 W/m², at 25°C. At 100 and 500 W/m², PV farm provides a maximum power of approximately 28 kW and 145 kW, respectively. At the irradiance of 1000 W/m², results are similar to the maximum performance of the previous plot at 25°C, which is the PV farm best perfomance operation point.

Lastly, DC voltage is converted to AC voltage of 250 V by the inverter. For this, a standard power and current controller was adopted, considering gains and constants from [20].

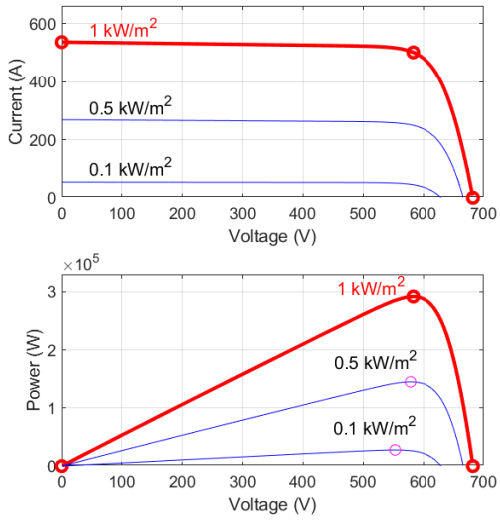

Fig. 7. PV farm performance curves according irradiance variation.

B. Model simulation

Simulations were performed in Simulink where the model was composed by standard blocks and blocks from the Specialized Power Systems library, contained in the Simscape Electrical section. Considering the simulation type, the discretization of the electrical system was adopted for a solution at fixed time steps. The converters blocks just work at discrete time solver. In this case, the step time of the electrical device blocks was 50.5 μs for the discrete time sumulations.

As for the Load Flow Analizer tool, responsible for determining the initial conditions of some parameters, the maximum number of iterations of 50, the frequency of 60 Hz, the base power of 250 kW and the voltage and power units in kV and kW.

For the general Simulink solver, the step time of 5.05 μs and the 4th order Rugge-Kutta method were considered.

VI. SIMULATION RESULTS

The grid model was simulated in Simulink and the following measurements at Bus 2 were performed during all tests in order to analyze and compare them: active and reactive power, RMS three-phase grid voltage and frequency. According to [13], thermal generation machines systems usually have inertia constants (H) from 1 to 10 s, depending on the system. With the purpose of verifying the action of the emulated inertia, it is suggested that comparisons be made among the scenarios in Table I.

First, the analysis of the adopted model is performed. For testing simulated system dynamics in each scenario, the following actions were performed on the grid when in steady state at nominal operation: frequency variation imposition, active power reference change, load variation and high level frequency variation with a limitation system. In all tests, was considered a PV solar active power generation reference of 0.95 pu as initial condition and a constant reactive power reference of zero pu, for a 250 kVA base power. The base voltage is 25 kV at the measured bus. For this, it is considered that during the simulations there is an average solar irradiance of 1000 W/m² and the temperature in the solar modules is 25 °C, which means that the solar farm is able to provide the nominal power. However, if conditions are not favorable to generate nominal power, the power reference is reduced according to what the system can provide.

TABELA I
Simulation scenarios

Scenario	Vitual inertia constant
1	No inertia (H = 0 s)
2	H = 1 s
3	H = 5 s
4	H = 10 s

For the time constant T_{VI} of the inertia controller, a value of 0.1 was selected empirically in order to filter out eventual impulses and noise from the measured RoCoF, without filtering the expected variations of this derivative. Therefore, with this constant, the controller has the characteristic of a low-pass filter with a cutoff frequency of 10 rad/s.

A. System model analysis

The EPS object of this study was linearized by the Simulink through the Model Linearizer tool. For linearization, the active power reference block was selected as the system input and the frequency, grid voltage and active and reactive power responses were selected as output. Correct linearization is performed considering the operating point. The operating point considered for simulations was the active power reference of 0.95 pu, frequency of 1.0 pu, measured active power of 0.95 pu and reactive power of zero pu. After running the Model Linearizer tool, Simulink gives all the eigenvalues (poles) of the linearized system and its dominant poles are demonstrated in Table II. In all scenarios there is the same real dominant pole of -1.31. What changes among one case and another are the complex conjugate poles responsible for the oscillations.

Considering the complex poles conjugated with frequencies close to 897.6 Hz in scenario 1 and 907.2 Hz in scenario 2, it is noted that the biggest difference between them is the damping ratio, which in scenario 2 is higher (12 .7% against 8.08%) . This means that the system with an inertia constant of 1 s is more damped than the system without any inertia emulation.

Comparing scenario 2 with scenario 3, in the latter there are complex poles conjugated at a frequency of 350.1 Hz with a damping rate of 50.95%, which is much higher than any damping provided by scenario 2.

The poles contained in the 921.5 Hz frequency of scenario 3 have a damping ratio of 15.4%, while at practically the same frequency as in scenario 4 (927.9 Hz) the poles have the highest

damping ratio (17.8%).

TABELA II
System modal analysis

Scenario	Natural frequency (Hz)	Damping ratio (%)	Eigenvalues
1	0.21	100	-1.31
	897.6	8.08	-455 ± j5620
	900.8	13.3	-755 ± j5610
2	0.21	100	-1.31
	822.8	12.7	-657 ± j5130
	907.2	12.4	-707 ± j5660
3	0.21	100	-1.31
	350.1	50.95	-1120 ± j1900
	921.5	15.4	-894 ± j5720
4	0.21	100	-1.31
	927.9	17.8	-1040 ± j5740
	1072.7	8.12	-547 ± j6710

Thus, the analysis of the system poles shows that higher inertia constants applied to the system result in more dampened systems.

B. Frequency variation response

The first test performed was the forced change of the grid frequency imposed by the infinite bus to simulate a power imbalance and verify the action of the inertia controller according to the swing equation. Therefore, the frequency variation from 60 to 61 Hz in a 0.5 second duration ramp was applied, considering the system in nominal steady state as initial condition. In this case, the inertia controller is expected to reduce the generated power reference while the frequency has positive variation. The responses are illustrated in Fig. 8.

First, the frequency variation imposed by the infinite bus is shown in Fig. 8.d. The plot contained in Fig. 8.a demonstrates the comparison among the variations in active power generated for each scenario. In all active power curves, power decreases only during the positive variation of the frequency, returning to the power of 0.95 pu after 2.5 s. For the largest inertia constant (scenario 4), there is the largest power variation of -0.095 pu (-10%). This reduction is a consequence of the P_{VI} power signal provided by the inertia controller with the maximum value of 0.11 pu (see Fig. 8.e). However, the generated power only did not reduce 0.11 pu because there was not enough time for it to reach steady state and this applies to all scenarios with constant inertia different from zero. In scenario 3, the active power reaches the minimum value of 0.9 pu (-4.7%), resulting from the maximum P_{VI} power value of 0.055 pu. In scenario 2 (minor inertia constant), there is the smallest difference in relation to the power generated in scenario 1 (no inertia), as expected. Hence the active power of scenario 2 reaches the minimum value of

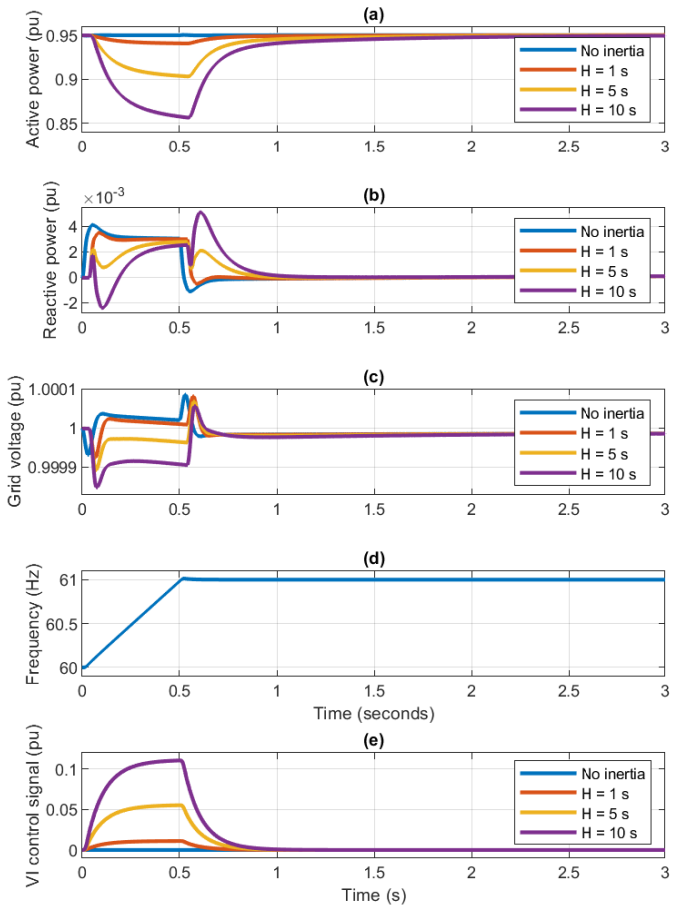

Fig. 8. Responses during a frequency deviation.

0.94 (around -1%) with a maximum P_{VI} signal of 0.011 pu. In scenario 1, active power is controlled only by conventional inverter control without inertia emulation and remains constant during any frequency variation. Therefore, the inertia controller is performing as expected and as it is determined by the swing equation. While the frequency is constant, it means that there is no imbalance between the generated and consumed active powers and the virtual inertia controller does not need to act.

Reactive powers (see Fig. 8.b) and, consequently, grid voltages (Fig. 8.c) present a very small variation. Among all cases, the reactive power has a zero steady state value at the beginning and end of the transient and reaches the lowest minimum value of -2.2x10^{-3} pu after frequency starts its positive variation in scenario 4 (largest inertia constant), and the maximum value of 4.7x10^{-3} pu when the frequency stabilizes in the same scenario. The grid voltages, on the other hand, has a voltage of virtually 1 pu in steady state and the highest variation of 150x10^{-6} pu, which is practically negligible. Therefore, grid voltage remains stable without significant influence from the inertia controller, which also occurs due to the preponderance of the infinite bus.

C. Generated power reference change

In the second test applied, the generated power reference was changed from 0.95 pu in steady state to 0.9 pu in a time equal to zero seconds of simulation. This test is equivalent to changing the reference power provided by the secondary frequency control. According to the swing equation, the reduction of generated active power implies a negative frequency variation, which can be verified in the results presented in the plot in Fig. 9.a. However, due to the frequency imposition of the infinite bus, the influence of the generated power variation results in very small frequency variation. Thus, it is difficult to verify the amplitude difference among the curves of the signals generated in each scenario. In order to see the differences, the curve equivalent to the frequency curve of scenario 1 (no inertia) minus the curve of each scenario with inertia emulation was calculated and ploted (see Fig. 9.b). This means that the response curve of the system without inertia (scenario 1) is the reference. In this case, the greater the difference, the further away from the reference curve the measured signal is. The same procedure was done for power and voltage measurements on the grid.

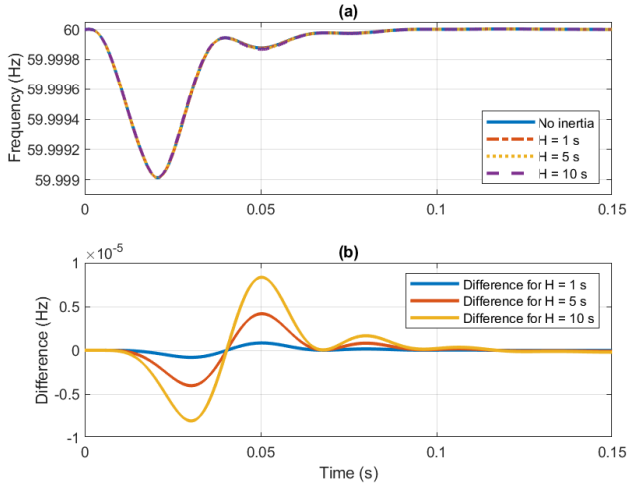

Fig. 9. Frequency response and differences after active power reference change.

After changing the generated active power reference, the average frequency variation between the scenarios was approximately -1x10^{-3} Hz. As the frequency corresponding to scenario 1 has a greater range of variation, it can be seen that in scenario 4 (largest inertia constant) the frequency presented a maximum variation approximately 0.8x10^{-5} Hz smaller compared to the system without inertia, due to the effect of the emulated inertia. Likewise, the frequency corresponding to scenario 3 presented maximum variation 0.4x10^{-5} Hz smaller than scenario 1. In scenario 2, the maximum difference was only 0.06x10^{-5} Hz. In Fig. 10, the results of the variation of active power generated measured in Bus 2 are presented.

Active power curves from all scenarios are shown in Fig 10.a.

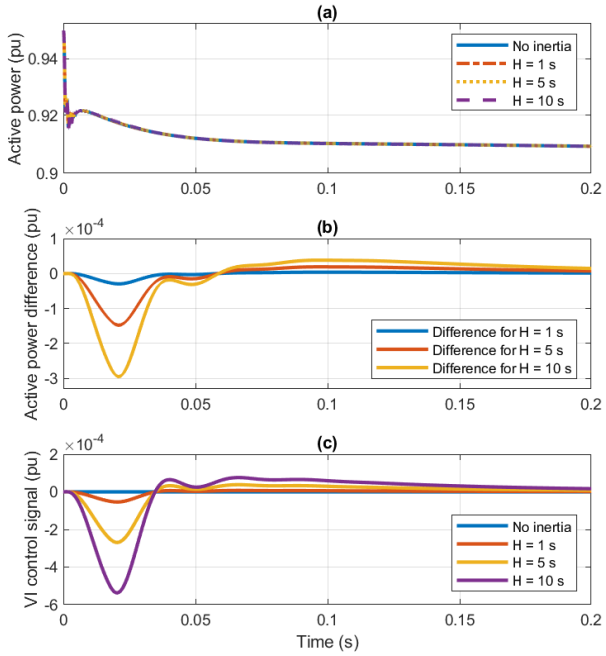

Fig. 10. Active power response and differences after active power reference change.

The graph displays responses up to a time of 0.2 s, however, the power reaches steady state value after approximately 2.5 s. In Fig. 10.b, the differences among the active power oscillations generated during the frequency variation are presented. In scenario 4 there was the greatest maximum power variation resulting from the emulated inertia, compared to the system without inertia, around 2.8x10^{-4} pu. This value is caused by the maximum variation of the P_{VI} inertia control signal of -5.2x10^{-4} pu (see Fig 10.c).

Fig. 11 displays grid voltage response and differences after the generated active power change.

In Fig 11.a, it is possible to see the initial oscillation that occurs in all scenarios, where the voltage reaches the minimum value of 1.00025 pu. However, in Fig. 11.b it is possible to see that the greatest voltage variation occurs in scenario 1 with the maximum difference of 10x10^{-7}pu compared to scenario 4.

Therefore, after changing the generated active power reference value, the emulated inertia imposed itself against active power variation.

D. Load variation

The variation of the consumed power was the third test applied. In this case, a load reduction of 200 kW on Bus 5 was carried out, in which the load of 2 MW was changed to 1.8 MW in form of a negative step. According to the swing equation, contrary to the reduction of the active power generated, it is expected that frequency presents a positive variation. The frequency response curves and differences of each scenario with

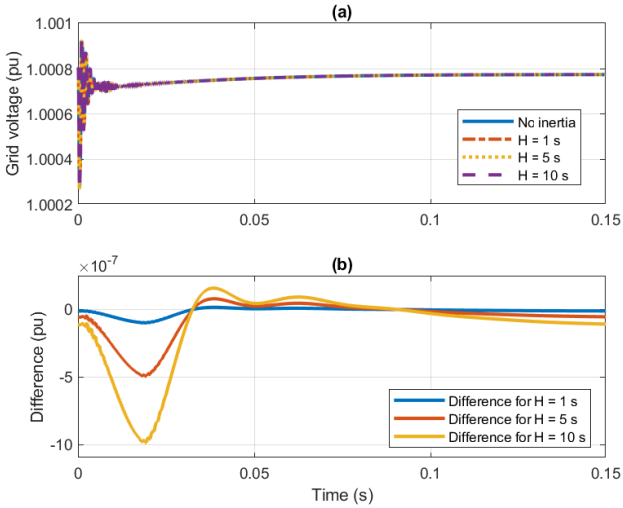

Fig. 11. Grid voltage response and differences after active power reference change.

emulated inertia compared to scenario 1 are shown in Fig. 12.

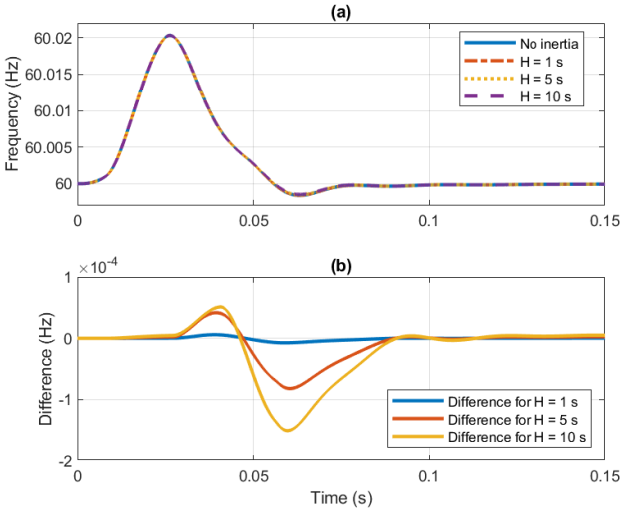

Fig. 12. Frequency response and differences after load reduction.

As can be seen in Fig. 12.a, the frequency presented the maximum positive overall variation of 0.02 Hz after load reduction. The smallest variation in frequency amplitude occurred in scenario 4, in which the emulated inertia acted with the greatest intensity and presented the maximum difference of -15x10^{-5} Hz compared to the system without inertia (see Fig. 12.b).The measured active power responses after load reduction are displayed in the graphs in Fig. 13.

In the case of load reduction, active power has more oscillatory responses than the previous tests, as shown in Fig. 13.a. This oscillation, that occurs just after load disconnection, is due to system characteristics seen from Bus 5. The oscillation exhibits the overall maximum

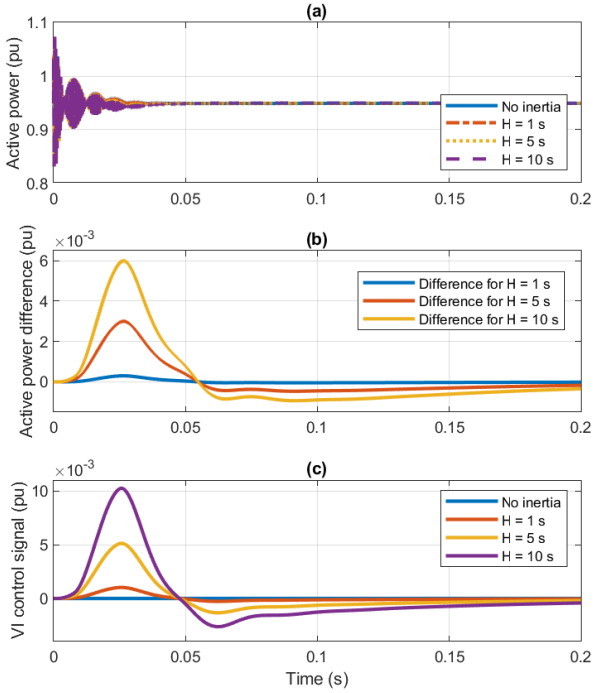

Fig. 13. Active power response and differences after load reduction.

amplitude of approximately 1.07 pu. The maximum difference for scenario 4 is 6x10^{-3} pu (Fig. 13.b) resulting from the higher P_{VI} signal amplitude, which is around 10x10^{-3} pu (Fig. 13.c). Grid voltage curves are illustrated in Fig. 14.

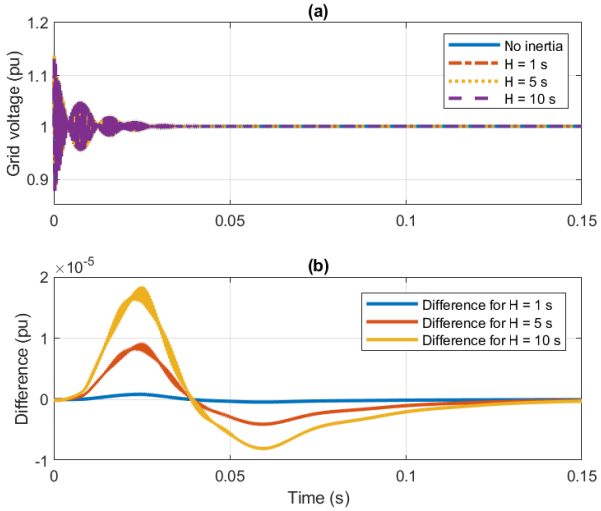

Fig. 14. Grid voltage response and differences after load reduction.

Grid voltage has initial oscilations as well, as indicated in Fig. 14.a. The maximum value is 1.14 pu in this case with the maximum difference of 1.8x10^{-5} (Fig. 14.b) in scenario

4. Again, the voltage does not show significant fluctuations while virtual inertia is acting due to the imposition of infinite bus voltage. However, the responses demonstrate the action of the emulated inertia even with low amplitude.

E. High level frequency variation

Finally, it is suggested to implement a shutdown system for the inertia emulation control, in cases of sudden high frequency variations. Hence a high level RoCoF results in a high power variation during the transient and this can make the system work outside the linear operating region. Inertia control is not intended to control high frequency variations caused by events such as a short circuit, for example. Thus, to prevent the inertia control from destabilizing the system in this case, it was implemented a structure that disables the inertia control when it makes the generated power reaches certain pre-defined limits.

To carry out the tests, scenario 4 was considered, in which there is a greater inertia constant (H = 10 s) and, therefore, a major variation in active power during frequency variation. To verify the right operation of the VI control switching system, the generated active power limits of ±10, ±20 and ±30% from nominal value were considered. As a disturbance, a variation of 5 Hz in a decreasing ramp that lasts for 0.42 seconds was applied by the infinite bus power grid when the PV solar active power was in steady state of 0.95 pu. Fig. 15 contains all graphical results.

In Fig. 15.a it is possible to observe that power started to rise due to the influence of the P_{VI} signal (Fig 15.d). However, the inertia control was disabled as soon as each active power reached the stipulated limit. This was due to feedback from the inertia control signals being disconnected from the active power control reference. The switched P_{VI} signals are shown in Fig. 15.e. In this case, the voltage presented a more accentuated oscillation due to the high frequency variation, reaching the minimum value of 0.97 pu when the 30% limit of active power was reached.

Therefore, the inertia control switching system worked as expected in order to mitigate the possibility of destabilization of the EPS in question.

VII. CONCLUSION

In this paper it was considered the problem caused by the low inertia of renewable energy sources interfaced by inverters when connected to the grid. To mitigate this problem, it was proposed to implement an inertia emulation control strategy, based on the swing equation, in a grid-following inverter connected to a photovoltaic solar source. The virtual inertia generation system was applied via simulation in an adapted SMIB system to prove its operation. The results demonstrate that this type of inertia emulation control is effective in controlling frequency stability considering low RoCoF values. Although the infinite bus imposes the voltage and frequency of the grid, the implemented virtual inertia was able to show results that demonstrate its action in controlling stability. Furthermore, the application of the limiter for the linear operating region proved to be effective,

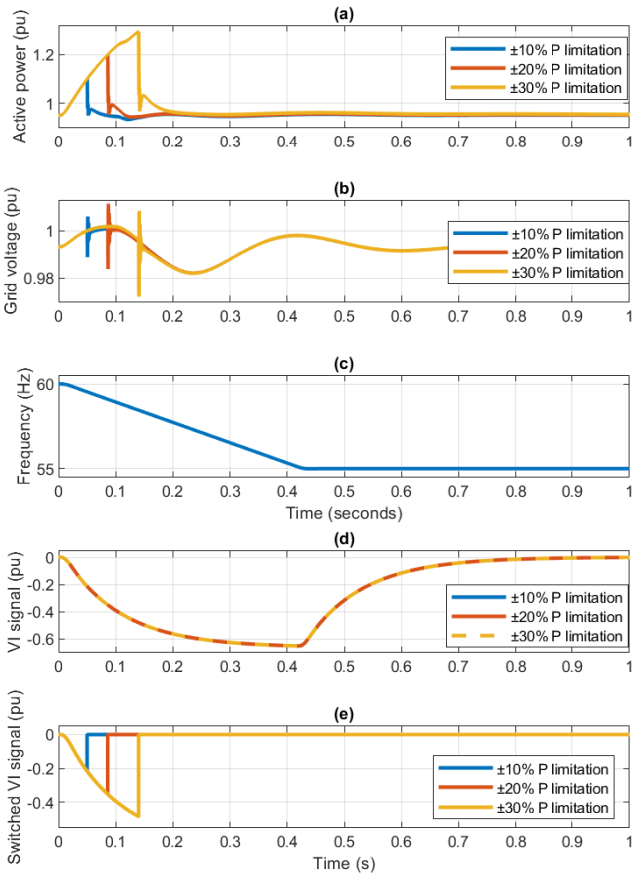

Fig. 15. Responses during a high frequency deviation.

preventing the system from becoming unstable when there were large frequency variations. Therefore, the applied tests provided expected results in the question of active power transfer and inertial response dictated by the swing equation.

As a suggestion for future implementations, the implementation of VI-based grid-following in an islanded EPS is proposed to verify its performance when connected to a grid more susceptible to frequency variations.

REFERÊNCIAS

[1] Q.-C. Zhong, G. Weiss, "Synchronverters: Inverters That Mimic Synchronous Generators", *IEEE Transactions on Industrial Electronics*, vol. 58, no. 4, pp. 1259–1267, 2011, doi:10.1109/TIE.2010.2048839.

[2] H. Zsiborács, N. Hegedűsné Baranyai, A. Vincze, L. Zentkó, Z. Birkner, K. Máté, G. Pintér, "Intermittent Renewable Energy Sources: The Role of Energy Storage in the European Power System of 2040", *Electronics*, vol. 8, p. 729, 06 2019, doi:10.3390/electronics8070729.

[3] B. Kroposki, B. Johnson, Y. Zhang, V. Gevorgian, P. Denholm, B.-M. Hodge, B. Hannegan, "Achieving a 100% Renewable Grid: Operating Electric Power Systems with Extremely High Levels of Variable

Renewable Energy", *IEEE Power and Energy Magazine*, vol. 15, no. 2, pp. 61–73, 2017, doi: 10.1109/MPE.2016.2637122.

[4] M. P. Musau, T. L. Chepkania, A. N. Odero, C. W. Wekesa, "Effects of renewable energy on frequency stability: A proposed case study of the Kenyan grid", *in 2017 IEEE PES PowerAfrica*, pp. 12–15, 2017, doi: 10.1109/PowerAfrica.2017.7991192.

[5] D. Orihara, H. Kikusato, J. Hashimoto, K. Otani, T. Takamatsu, T. Oozeki, H. Taoka, T. Matsuura, S. Miyazaki, H. Hamada, K. Mori, "Contribution of Voltage Support Function to Virtual Inertia Control Performance of Inverter-Based Resource in Frequency Stability", *Energies*, vol. 14, no. 14, 2021, doi:10.3390/en14144220, URL: https://www.mdpi.com/1996-1073/14/14/4220.

[6] European Network of Transmission System Operators for Electricity, *Inertia and Rate of Change of Frequency*, Version 17, Belgium, 2020.

[7] P. Tielens, D. Van Hertem, "The relevance of inertia in power systems", *Renewable and Sustainable Energy Reviews*, vol. 55, pp. 999–1009, 03 2016, doi: 10.1016/j.rser.2015.11.016.

[8] F. Milano, F. Dörfler, G. Hug, D. J. Hill, G. Verbič, "Foundations and Challenges of Low-Inertia Systems (Invited Paper)", *in 2018 Power Systems Computation Conference (PSCC)*, pp. 1–25, 2018, doi:10.23919/PSCC.2018.8450880.

[9] S. J. Chapman, *Electric Machinery Fundamentals*, 5 ed., McGraw-Hill Education, New York, 2012.

[10] K. Y. Yap, C. R. Sarimuthu, J. M.-Y. Lim, "Virtual Inertia-Based Inverters for Mitigating Frequency Instability in Grid-Connected Renewable Energy System: A Review", *Applied Sciences*, vol. 9, no. 24, 2019, doi:10.3390/app9245300, URL: https://www.mdpi.com/2076-3417/9/24/5300.

[11] B. K. Poolla, D. Groß, F. Dörfler, "Placement and Implementation of Grid-Forming and Grid-Following Virtual Inertia and Fast Frequency Response", *IEEE Transactions on Power Systems*, vol. 34, no. 4, pp. 3035–3046, 2019, doi:10.1109/TPWRS.2019.2892290.

[12] J. Machowski, J. W. Bialek, J. R. Bumby, *Power System Dynamics: Stability and Control*, 2 ed., Chichester, U.K.: Wiley, 1997.

[13] P. Kundur, N. Balu, M. Lauby, *Power system stability and control*, vol. 23, McGraw-Hill Education, New York, 1994.

[14] P. Roos, "A Comparison of Grid-Forming and Grid-Following Control of VSCs", *Dissertation*, 2020.

[15] Z. Alqarni, J. A. Asumadu, "A Synchronized Grid Integrated Three-Phase Inverter with a Renewable Source for Power Sharing", *Journal of Power and Energy Engineering*, vol. 8, pp. 88–101, 2020, doi: 10.4236/jpee.2020.83006.

[16] V. Skiparev, R. Machlev, N. R. Chowdhury, Y. Levron, E. Petlenkov, J. Belikov, "Virtual Inertia Control Methods in Islanded Microgrids", *Energies*, vol. 14, no. 6, 2021, doi:10.3390/en14061562, URL: https://www.mdpi.com/1996-1073/14/6/1562.

[17] B. Behar, F. Lamnabhi-Lagarrigue, T. Ahmed-Ali, "Robust nonlinear control of transient stability of power systems", vol. 1, pp. 294 – 299 Vol.1, 01 2004, doi: 10.1109/CDC.2003.1272576.

[18] MathWorks, "250-kW Grid-Connected PV Array", , 2021.

[19] SolarHub, "PV Module SPR-415E-WHT-D Details", , 2021.

[20] VDI/VDE, *Guidelines for testing control systems of steam turbines - Dynamic behavior of speed and load control*, Sheet 4 VDI/VDE 3521, Verein Deutscher Ingenieure - VDI Std, 2000.

YURI ROBERTO FERREIRA

Control strategy to emulate inertia through grid-following inverter
(Estratégia de controle para emulação de inércia através de inversores seguidores de rede).

Este trabalho foi julgado adequado para obtenção do título de Bacharel em Engenharia Elétrica, pelo Instituto Federal de Educação, Ciência e Tecnologia de Santa Catarina, e aprovado na sua forma final pela comissão avaliadora abaixo indicada.

Jaraguá do Sul, 18 de Agosto de 2021

_____
Prof. Dr. Rodrigo Trentini Preuss
Orientador
IFSC – Campus Jaraguá do Sul – Rau

_____
Prof. MSc John Jefferson Antunes Saldanha
IFSC – Campus Jaraguá do Sul – Rau

_____
Prof. Dr. Moisés Ferber
UFSC - Campus Joinville

_____
Prof. Dr. Rodrigo Trentini Preuss
IFSC – Campus Jaraguá do Sul – Rau

#284e8e4c-708c-45ff-ae6d-c28ff85710f4

Comprovante de Assinatura Eletrônica

contraktor

Datas e horários baseados no fuso horário (GMT -3:00) em Brasília, Brasil
Sincronizado com o NTP.br e Observatório Nacional (ON)
Certificado de assinatura gerado em 19/08/2021 às 10:56:15 (GMT -3:00)

TermoDeAprovacao_TCC_EngEletrica_IFSC_JGS_RAU_18082021_YuriRobertoFerreira.docx.pdf

ID única do documento: #284e8e4c-708c-45ff-ae6d-c28ff85710f4

Hash do documento original (SHA256): aba60939978a7cbdb75aff744db7cb63069c5141f0533ef0e1e61c8a157e3fe8

Este Log é exclusivo ao documento número #284e8e4c-708c-45ff-ae6d-c28ff85710f4 e deve ser considerado parte do mesmo, com os efeitos prescritos nos Termos de Uso.

Assinaturas (4)

- Moises Ferber (Participante)
  Assinou em 21/08/2021 às 09:21:04 (GMT -3:00)
- Rodrigo Trentini Preuss (Participante)
  Assinou em 19/08/2021 às 11:05:06 (GMT -3:00)
- John Jefferson Antunes Saldanha (Participante)
  Assinou em 19/08/2021 às 11:04:30 (GMT -3:00)
- Rodrigo Trentini Preuss (Participante)
  Assinou em 19/08/2021 às 10:59:02 (GMT -3:00)

Histórico completo

Data e hora	Evento
21/08/2021 às 09:21:04 (GMT -3:00)	Moises Ferber (Autenticação: e-mail moises.ferber@ufsc.br; IP: 177.204.46.151) assinou. Autenticidade deste documento poderá ser verificada em https://verificador.contraktor.com.br. Assinatura com validade jurídica conforme MP 2.200-2/01, Art. 10o, §2.

Data e hora	Evento
19/08/2021 às 11:04:30 (GMT -3:00)	John Jefferson Antunes Saldanha (Autenticação: e-mail john.saldanha@ifsc.edu.br; IP: 131.100.95.17) assinou. Autenticidade deste documento poderá ser verificada em https://verificador.contraktor.com.br. Assinatura com validade jurídica conforme MP 2.200-2/01, Art. 10o, §2.
19/08/2021 às 10:59:02 (GMT -3:00)	Rodrigo Trentini Preuss (Autenticação: e-mail rodrigo.trentini@gmail.com; IP: 190.102.49.159) assinou. Autenticidade deste documento poderá ser verificada em https://verificador.contraktor.com.br. Assinatura com validade jurídica conforme MP 2.200-2/01, Art. 10o, §2.
19/08/2021 às 11:05:06 (GMT -3:00)	Rodrigo Trentini Preuss (Autenticação: e-mail rodrigo.trentini@ifsc.edu.br; IP: 190.102.49.159) assinou. Autenticidade deste documento poderá ser verificada em https://verificador.contraktor.com.br. Assinatura com validade jurídica conforme MP 2.200-2/01, Art. 10o, §2.
19/08/2021 às 10:56:19 (GMT -3:00)	Rodrigo Trentini Preuss solicitou as assinaturas.
21/08/2021 às 09:21:05 (GMT -3:00)	Documento assinado por todos os participantes.

RESOLUÇÃO Nº 11/2021/Colegiado Jaraguá do Sul, 27 de maio de 2021.

Dispõe sobre a autorização de excepcionalidade para realização de Trabalho de Conclusão de Curso em língua inglesa no curso Bacharelado em Engenharia Elétrica do Câmpus Jaraguá do Sul – Rau.

O PRESIDENTE DO COLEGIADO DO IFSC CÂMPUS JARAGUÁ DO SUL – RAU, órgão superior de caráter normativo e deliberativo no âmbito do Câmpus por atribuição do CONSUP, no uso das atribuições que lhe foram conferidas pela Portaria Nº 1.638 de 30/04/2020;

Considerando a 3ª Reunião Ordinária do Colegiado do câmpus Jaraguá do Sul – Rau, realizada em 25 de maio de 2021;

RESOLVE:

Art.1º Autorizar a excepcionalidade para redação e apresentação do Trabalho de Conclusão de Curso em língua inglesa para o aluno Yuri Roberto Ferreira, matrícula 201810205138, do curso Bacharelado em Engenharia Elétrica no câmpus Jaraguá do Sul – Rau.

Art. 2º Esta resolução entra em vigor a partir de sua publicação.

Publique-se e
Cumpra-se.

DELCIO LUÍS DEMARCHI
Presidente do Colegiado do Câmpus Jaraguá do Sul – Rau/IFSC
Autorizado conforme despacho no documento nº 23292.014653/2021-63